http://ansinet.com/itj

ITJ

ISSN 1812-5638

INFORMATION TECHNOLOGY JOURNAL

ANSInet
Asian Network for Scientific Information
308 Lasani Town, Sargodha Road, Faisalabad - Pakistan

Information Technology Journal 10 (4): 736-747, 2011
ISSN 1812-5638 / DOI: 10.3923/itj.2011.736.747

Fuzzy Sliding-mode Control for the Swing Arm Used in a Fourier Transform Spectrometer

Shi Yufeng, Zhou Chunjie and Liao Zheng
Key Laboratory of Ministry of Education for Image Processing and Intelligent Control,
Department of Control Science and Engineering, Huazhong University of Science and Technology,
1037 Luoyu Road, Wuhan, Hubei, 430074, China

Abstract: This study presents a Fuzzy Integral Sliding-Mode Control (FISMC) approach for the high precision motion control of Fourier Transform Spectrometer (FTS) based on Michelson interferometer. In this motion system, the system parameters are nonlinear and time-varying because of the mechanical design. To deal with these problems, a new control strategy which implies a FISMC for the speed loop and a Proportional-Integral (PI) control for the current loop is used to track the desired Optical Path Difference Velocity (OPDV) accurately. A Sliding-Mode Control (SMC) is designed to enhance the robustness of the system and reduce the influences of the time-varying disturbances. The integral in the sliding-mode surface is utilized to reduce the steady-state tracking error. Moreover, a fuzzy logic controller is served as a gain factor to suppress the undesired chattering introduced by SMC for the steady tracking. Finally, simulation and experimental results demonstrate the effectiveness of the proposed FISMC for the precision control of FTS.

Key words: Swing arm, voice coil motor, SMC, fuzzy control, parameter variation

INTRODUCTION

Fourier Transform Spectrometer (FTS) based on Michelson interferometer is widely used in petroleum chemicals, biotechnology, spectral analysis and space exploration, for the advantages of high luminous flux and spectral resolution (Steck and von Clarmann, 2001; Friedl-Vallon *et al*., 2004). However, the spectral resolution is easily influenced by the Signal-to-Noise-Rate (SNR) in the system. Hence, a precise scanning mechanism and highly stable control strategy for the movable mirror are necessary in these instruments for the purpose of reducing the sampling noises (Zachor, 1977; Comolli and Saggin, 2005). In addition, a fast regulating is needed for maximizing the effective Optical Path Difference (OPD) in a limited space. In this study, the FTS is designed in the rotary way. There is a cosine relationship between the OPDV on the tangential direction of the circular motion and the angular velocity of the Voice Coil Motor (VCM). Hence, the parameters of the system are time-varying. Moreover, the load of the system is also time-varying due to the flexure pivot, which is the disturbance for control. As the foregoing disadvantages, it is difficult to ensure a high precision control for the scanning. Furthermore, the space environment where the FTS is applied introduces a micro-vibration disturbance to the system load. Therefore, the motivation of this study is to design a suitable control strategy to overcome these limitations.

The Proportional-Integral-Differential (PID) control which is applied extensively in the industry field is simply and easily implemented in deterministic systems, but it is difficultly to be employed in uncertain systems. The Sliding-Mode Control (SMC) which is a nonlinear robust control approach is widely used in motor drives. Its great advantage is that an accurate system model is not needed (Lai and Shyu, 2005; Barambones *et al*., 2007). It is especially suitable for the systems with time-varying parameters or external disturbances, even for the nonlinear systems. Under the SMC, the system is constrained to move along the designed sliding-mode surface with high-frequency discontinuous switching which is called sliding-mode. Designing an opportune sliding-mode surface except the variable parameters and interferences of the system, it is insensitive to the variations of the system parameters and external disturbances (Spurgeon, 1991). However, the robustness of the system is not guaranteed before the system comes into the sliding-mode. If there are some load disturbances in the system, they may result in a steady-state error with this control strategy (Jiao and Luo, 2009). For these problems, an integral compensator is added to the sliding-mode surface. It can guarantee a global robustness throughout the entire responses of the

Corresponding Author: Zhou Chunjie, Key Laboratory of Ministry of Education for Image Processing and Intelligent Control, Department of Control Science and Engineering, Huazhong University of Science and Technology, 1037 Luoyu Road, Wuhan, Hubei, 430074, China Tel: +86 027 87558001 Fax: +86 027 87543230

system. Chern and Wu (1991) designed a variable structure control for an electrohydraulic position servo control system. With the integral compensator, it achieved accurate servo tracking in the presence of load disturbance and plant parameter variation. Although a high-frequency switching can increase the robustness of the system, the undesired chattering is unavoidable in the conventional SMC, which may excite a high-frequency response and limit its applications (Koshkouei *et al*., 2005). Furthermore, the bounds of uncertainties are also needed in SMC.

Fuzzy logic has the ability to express the amount of ambiguity as human think. Its features are good self-adaptability and strong structure robustness, but the fuzzy rules are too complex for some applications (Wai *et al*., 2008). Combining with the SMC, the fuzzy rules can be reduced and the chattering phenomenon can be suppressed intellectually and self-adaptively. Nowadays, many studies have focused on utilizing the advantages of fuzzy logic and SMC for motor control. Wai and Su (2006) proposed an adaptive fuzzy enhanced sliding-mode control for an indirect field-oriented induction motor. A fuzzy hitting control was utilized to replace the hitting control for dealing with the chattering phenomena in the conventional SMC. However, its stable range did not contain the slip-frequency-estimation part. For the linear systems with mismatched time-varying uncertainties, an AFSMC was applied (Tao *et al*., 2003). With this strategy, the requirement of the available uncertainty bounds is not necessary. Although many literatures have been studied for estimating the uncertainties of the system online to suppress the chattering using fuzzy logic on the SMC, the study on combining the fuzzy logic and ISMC has not been fully explored.

This study proposes a novel double closed-loop control method with speed loop based on FISMC and current loop based on PI for accurate scanning and tracking control in the FTS. Combining the advantages of fuzzy logic and ISMC, it can reduce the steady-state error effectively and suppress the chattering phenomena self-adaptively. The robustness of the system against the parameter variations and load disturbances can also be increased observably. In order to track the desired OPDV stably, the system is modeled with the error of OPDV and its differential coefficient. Different from the conventional integral sliding-mode surface, a new surface is designed with the feedback of the system, its error, integral and differential coefficient. And this new surface is used as the input of the fuzzy logic control. The output of the fuzzy logic is applied as a regulatory factor for the switching control of the ISMC. With this design, the complexities of the fuzzy rules and reasoning are reduced. Finally, the tracking of the desired OPDV is achieved with a high stability in the experiment, which is more than 99.1%.

PROBLEM STATEMENT

System formulation: The proposed FTS is mainly composed of Michelson interferometer, reference laser, photoelectric detector and spectral analysis, which is shown in Fig. 1. Two corner-cube mirrors are mounted at the edge of the swing arm. The incident light is split into two optical paths by the beam-splitter, one is the reflected light and the other is the transmitted light. The former reaches the bottom corner-cube mirror and retraces its path to the splitter by the top end mirror. The latter transmits to the opposite corner and also reflects back to the splitter. Then the interference is produced. By swinging the arm around the pivot at the wedge splice with the VCM, the OPD is changed and the interferogram is created at the splitter. Finally, the interferogram is sampled by the photoelectric detector. The spectrogram is acquired by inverse-Fourier-transforming with the sampled signals in the computer. Meanwhile, the reference laser beam which shares the same path with the incident light creates the laser interference with the varying of OPD. Then the interferogram of the reference laser is converted into a corresponding cosine function of the OPD by the photoelectric diode. A series of pulse signals which are generated at each zero crossing of the cosine signals (each zero crossing corresponds to a reference wavelength of the OPD), are used to trigger an equal optical path sampling and indicate the OPDV of the system as the feedback for the speed loop.

It is well known that the FTS is very sensitive to the stability of the OPDV. Although its sensibility can be reduced with the reference sampling, there are still some sampling errors when the OPDV is not a constant as there is a time lag between zero crossing and real sampling (Friedl-Vallon *et al*., 2004). According to the stability requirements of an interference spectrum, the error of the OPD within one period should be less than λ/SNR (Vaughan, 1989). It means that the stability of the OPDV should be more than 99% to satisfy the value of SNR being greater than 100. A high precision control is needed in this proposed design, which is a critical performance requirement.

Mathematical model of VCM: The motion system is mainly composed of the VCM, the swing arm, the flexure pivot and the pedestal. The VCM is a typical D.C. motor that is applied in many accurate positioning and precision

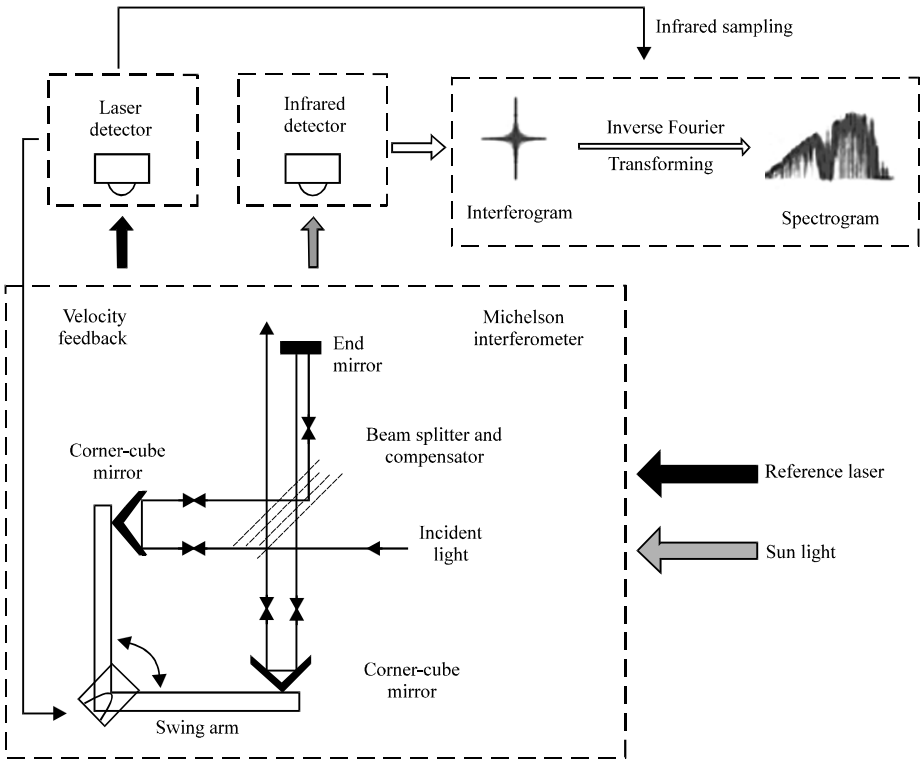

Fig. 1: Schematic diagram of the Fourier transform spectrometer

control fields for the advantages of fast response, no noise and high accuracy (Morcos, 1995). With the operating principle of the Lorentz force, the force acting on the rotor is proportional to the current applied in the coil, which is perpendicular to the directions of permanent magnetic field and current. By the circular arc air gap magnetic field designing, it provides rotary motion in a limited angle. According to the mechanical design, the arm is actuated to swing by the VCM with the rotor magnet fixed on it and the coil fixed on the pedestal as a stator. Then, the flexure pivot is chosen to connect the arm with the pedestal based on its negligible friction introducing a variation load. Hence, the friction is not taken into account the dynamic model of the VCM.

According to the Kirchhoff's Voltage Law, the voltage balance equation of the VCM is:

$$E = L\dot{i} + Ri + K_T\omega \quad (1)$$

And the moment equation is:

$$J_m\dot{\omega} = K_T i \quad (2)$$

where, E is the external supply, R is the resistance, L is the inductance of th e coil, i is the motor current, J_m is the moment of inertia for the coil, ω is the angular velocity, K_T is the motor torque constant.

As the load is a swing arm with a flexure pivot, its value of the elastic force is proportional to the pivot angle. The moment equation could be modified as:

$$J_\Sigma\dot{\omega} = K_T i - k\theta \quad (3)$$

where, θ is the swinging angle of the arm, k is the elastic coefficient of the pivot, $J_\Sigma = J_m + J_r$ is the moment of inertia which is the sum of the coil and arm.

From Eq. 3, the load of the VCM varies with the increasing or decreasing of swing angle due to the flexure pivot, which is a load disturbance for the servo control. It is a negative impact on the high precise control.

Nonlinear relationship between OPDV and angular velocity: According to the principle of equal OPD in the corner-cube mirror, the OPD between the two different positions of the corner-cube mirror is the length of arc caused by the swing of the arm. With the continuous motion of swing, the OPD is 8 times of the physical shift value of the corner-cube mirror, whose velocity is nonlinear relationship with the angular velocity of the motor as shown in Eq. 4.

$$\begin{cases}\omega = \dfrac{v}{8r\cos\theta} = \dfrac{v}{8r}\sec\theta \\ \theta = \int_0^t \omega dt\end{cases} \quad (4)$$

where, v is the OPDV, r is the length of the swing arm.

According to the design, the swing angle of the arm is limited in ±10°. The approximation of secθ at zero point based on Taylor Expansion is:

$$\omega \approx \frac{v}{8r}(1 + \frac{\theta^2}{2}) \quad (5)$$

Solve the Riccati Eq. 5, we can get:

$$\begin{cases}\theta = \sqrt{2}\,tg(\dfrac{\sqrt{2}}{2}At) \\ \omega = A\sec^2(\dfrac{\sqrt{2}}{2}At)\end{cases} \text{ where, } A = \frac{v}{8r} \quad (6)$$

From the equation above, one can get the angular velocity of the motor at a desired OPDV is:

$$\omega_0 = A_0\sec^2(\frac{\sqrt{2}}{2}A_0 t) \text{ where, } A_0 = \frac{v_0}{8r} \quad (7)$$

The angular velocity is a time-dependent variable shown as in Eq. 7, where, v_0 is the desired OPDV which is a constant, ω_0 is the corresponding angular velocity.

Similarly, the relationship between a small change of the OPDV and the corresponding change of the rotor angular velocity is:

$$\Delta\omega = \frac{\Delta v}{8r}\sec\theta = \frac{\Delta v}{8r}\lambda(t) \quad (8)$$

where, $\Delta\omega$ and Δv are the change of the rotor angular velocity and the OPDV, respectively, $\lambda(t)$ is the time-varying factor.

As the nonlinear relationship shown in Eq. 4, some time-varying parameters and uncertain disturbances are introduced to the control system, which are the challenges for the control design.

Control design for the swing arm: To achieve a swing motion at a stable and constant OPDV, a closed-loop control structure is designed in Fig. 2. The reference pulses into the QEP module of the DSP TMS320LF2407 are served as the feedback of OPDV in the speed loop, also used to indicate the position of the arm. The motor current is detected by a Hall sensor and inducted into the ADC through a low-pass filter as the current feedback in the current loop. An effective control algorithm is implemented in the DSP. The motor is driven by a bipolar PWM control circuit with the output of PWM from the DSP.

CONTROL ALGORITHMS AND IMPLEMENTATIONS

The double closed-loop control structure applied in the control algorithm is shown in Fig. 3. The outer speed loop is composed of a constant desired input of OPDV and the pulse feedback from the reference laser interference with photoelectric conversion. A PI control algorithm is adopted in the inner current loop, which is composed of the output of the speed loop and current feedback. The advantage of the former control law is to ensure a high stable OPDV and rapid response during the turning around of the arm, the latter is to achieve an error free tracking with the output of the speed loop and steady the output moment of the VCM for reducing the vibration of the arm.

The FISMC used in the speed loop is shown in Fig. 3. It combines both the advantages of fuzzy logic control and ISMC to increase the robustness of system against the time-varying load disturbance. In the part of ISMC, the integral sliding-mode surface is constituted by the feedback of OPDV, its error, integral and differential. In the section of fuzzy logic control, the input is the designed sliding-mode surface and the output is the gain factor for smoothing the sliding-mode switch process. Finally, the integral of the FISMC output is served as the input of the current loop.

The integral sliding-mode control: Considering the time-dependent relationship between OPDV and the angular velocity of motor, let the motor angular velocity, its first and second order derivatives be:

$$\begin{cases}\omega = \omega_0 - \Delta\omega \\ \dot{\omega} = \dot{\omega}_0 - \Delta\dot{\omega} \\ \ddot{\omega} = \ddot{\omega}_0 - \Delta\ddot{\omega}\end{cases} \quad (9)$$

Substitution of Eq. 9 into the derivation of Eq. 3 yields:

$$\begin{cases}\Delta\omega = \omega_0 - \omega \\ \Delta\ddot{\omega} = -\dfrac{k}{J_\Sigma}\Delta\omega - \dfrac{K_T}{J_\Sigma}\dot{i} + \dfrac{k}{J_\Sigma}\omega_0 + \ddot{\omega}_0\end{cases} \quad (10)$$

And the derivation of Eq. 8 is:

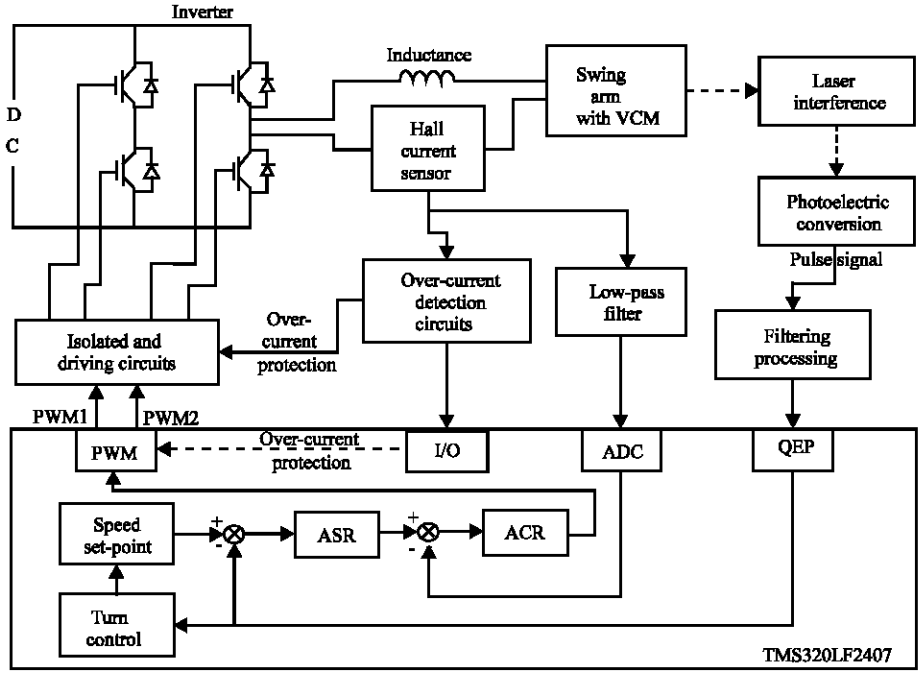

Fig. 2: Block diagram of the closed-loop control system

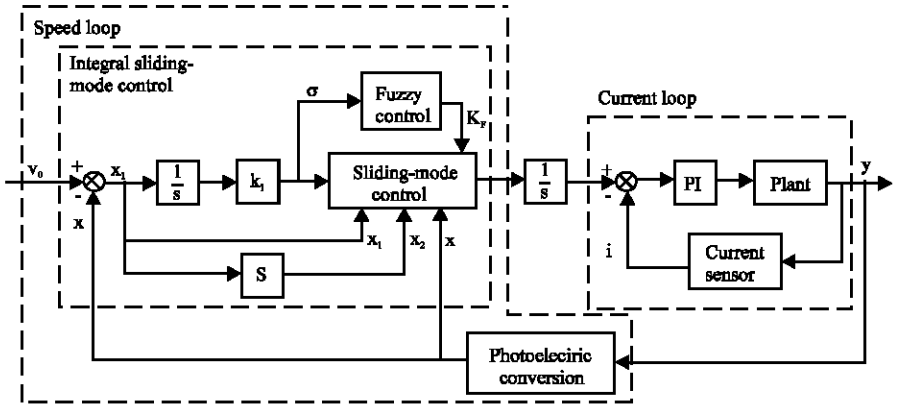

Fig. 3: Block diagram of speed-current double closed-loop control

$$\begin{cases}\Delta\dot{\omega} = \dfrac{\Delta\dot{v}}{8r}\lambda(t) + \dfrac{\Delta v}{8r}\dot{\lambda}(t)\\ \Delta\ddot{\omega} = \dfrac{\Delta\ddot{v}}{8r}\lambda(t) + 2\dfrac{\Delta\dot{v}}{8r}\dot{\lambda}(t) + \dfrac{\Delta v}{8r}\ddot{\lambda}(t)\end{cases} \tag{11}$$

According to the design with the constant OPDV as the desired input, we choose the error of OPDV and its first order derivative as the system state variables:

$$\begin{cases}\Delta v = x_1\\ \Delta\dot{v} = \dot{x}_1 = x_2\\ \Delta\ddot{v} = \dot{x}_2\end{cases} \tag{12}$$

Substituting Eq. 12 into Eq. 11, together with Eq. 8 and 10, one can get the system state equation as Eq. 13:

$$\begin{cases}\dot{x}_1 = x_2\\ \dot{x}_2 = (-\dfrac{k}{J_\Sigma} - \dfrac{\ddot{\lambda}(t)}{\dot{\lambda}(t)})x_1 - 2\dfrac{\dot{\lambda}(t)}{\lambda(t)}x_2 - \dfrac{K_T}{J_\Sigma}\dfrac{8r}{\lambda(t)}\dot{i} + \dfrac{8rk}{J_\Sigma\dot{\lambda}(t)}\omega_0 + \dfrac{8r}{\dot{\lambda}(t)}\ddot{\omega}_0\end{cases} \tag{13}$$

The double closed-loop control structure described in Fig. 3 implies that the output of the speed loop is the input of the current loop. Considering the parameter $\bar{i}$ is included in Eq. 13, let $\frac{8r}{\lambda(t)}\bar{i}$ be the output of FISMC in the speed loop and its integral be the input of the current loop. That is:

$$\begin{cases} u = \dfrac{8r}{\lambda(t)} i \\ f(t) = \dfrac{8rk}{J_\Sigma \lambda(t)} \omega_0 + \dfrac{8r}{\lambda(t)} \ddot{\omega}_0 \end{cases} \tag{14}$$

where, u is the output of the FISMC, f (t) is the nonlinear time-varying disturbance, ω_0 and $\ddot{\omega}_0$ are the time-dependent variable of the angular velocity and its second order derivative corresponding to the constant desired OPDV, respectively. Substitution of Eq. 14 into Eq. 13 yield:

$$\begin{cases} \dot{x}_1 = x_2 \\ \dot{x}_2 = (-\dfrac{k}{J_\Sigma} - \dfrac{\dot{\lambda}(t)}{\lambda(t)}) x_1 - 2\dfrac{\dot{\lambda}(t)}{\lambda(t)} x_2 - \dfrac{K_T}{J_\Sigma} u + f(t) \end{cases} \tag{15}$$

If there are some uncertain disturbances in the swing arm system, it could lead to steady-state error (Jiao and Luo, 2009). In order to reduce the steady-state error, a sliding-mode surface containing the integral of the error is introduced. Let the surface be:

$$\begin{cases} z = \int x_1 dt \\ \sigma = c_1(k_1 z - x) + c_2 x_1 + x_2 \end{cases} \tag{16}$$

where, z is the integral of error, x is the feedback of the OPDV, k_1 is integral gain, c_1 and c_2 are constant coefficients, σ is the sliding-mode switch function with error integral.

Let the output of the ISMC be:

$$u = u_s + u_{sw} \tag{17}$$

where, u_s is the proportional control with state variables, defined as:

$$u_s = \frac{(c_1 k_1 - \dfrac{k}{J_\Sigma}) x_1 + (c_2 - c_1) x_2}{K_T / J_\Sigma} \tag{18}$$

u_{sw} is designed for eliminating the interferences introduced by time-varying parameters or external disturbances and guaranteeing the sliding-mode motion of the system. It is constructed as follows:

$$u_{sw} = \varphi_1(k_1 z - x) + \varphi_2 x_1 + \varphi_3 x_2 + \varphi \mathrm{sgn}(\sigma) \tag{19}$$

where,

$$\varphi_1 = \begin{cases} \alpha_1 & \text{if} \quad (k_1 z - z)\sigma > 0 \\ \beta_1 & \text{if} \quad (k_1 z - z)\sigma < 0 \end{cases} \tag{20a}$$

$$\varphi_2 = \begin{cases} \alpha_2 & \text{if} \quad x_1 \sigma > 0 \\ \beta_2 & \text{if} \quad x_1 \sigma < 0 \end{cases} \tag{20b}$$

$$\varphi_3 = \begin{cases} \alpha_3 & \text{if} \quad x_2 \sigma > 0 \\ \beta_3 & \text{if} \quad x_2 \sigma < 0 \end{cases} \tag{20c}$$

$$\varphi = \begin{cases} \alpha & \text{if} \quad \sigma > 0 \\ \beta & \text{if} \quad \sigma < 0 \end{cases} \tag{20d}$$

The fuzzy logic control: The SMC theory implies that the robustness of the system against the disturbances and variable parameters could be increased with the switching control u_{sw}. However, the chattering phenomenon is unavoidable because of the high-frequency switching, which influences the stability of the system. Hence, fuzzy logic control is introduced into the SMC. By designing the appropriate control rules for fuzzy reasoning and using the output of fuzzy logic control as the regulatory factor for switching control, the system chattering could be suppressed. The output of the FISMC is modified as:

$$u = u_s + K_F u_{sw} \tag{21}$$

where, K_F is the output of the fuzzy logic control.

It is known that if the system is moving away the sliding-mode surface, which means $\sigma \neq 0$, then a larger change is needed to force it moving back to the surface; and when the system is moving on or at the vicinity of the surface, which means $\sigma \approx 0$, little change will be needed to keep its state of motion.

Define σ as the input of the fuzzy logic control. Then the fuzzy sets of the input and output can be defined, respectively, as:

$$\sigma = \{N\ Z\ P\}\ K_F = \{Z\ P\}$$

where, N represents the negative, Z represents the zero part, and P represents the positive.

The fuzzy rules for eliminating chattering are set as

- **Rule 1:** If σ is P, then K_F is P
- **Rule 2:** If σ is Z, then K_F is Z
- **Rule 3:** If σ is N, then K_F is P

According to the definitions above, the fuzzy universes of input σ and output K_F are defined, respectively, as:

$$\sigma = \{-600, -50, 0, 50, 600\}\ K_F = \{-0.6, 0, 0.6, 2.5\}$$

The membership functions of input σ and output K_F are shown in Fig. 4 and 5, respectively.

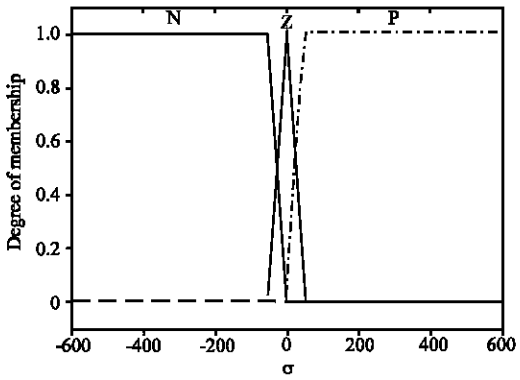

Fig. 4: Fuzzy input membership function

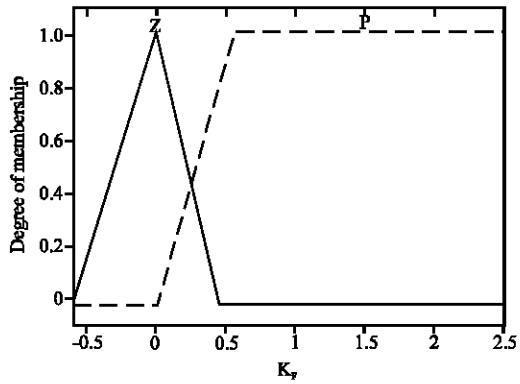

Fig. 5: Fuzzy output membership function

Stability of the control system: Define the Lyapunov candidate function as:

$$V = \frac{1}{2}\sigma^2 \tag{22}$$

After substituting Eq. 16 into Eq. 22, the derivation of the Lyapunov function with respect to time can be represented as:

$$\dot{V} = \sigma\dot{\sigma} = \sigma[c_1(k_1\dot{z} - \dot{x}) + c_2\ddot{x}_1 + \ddot{x}_2] \tag{23}$$

According to the relationship of the feedback, the desired OPDV and its error: $x = x_0 - x_1$, the derivation of this equation is:

$$\dot{x} = \dot{x}_0 - \dot{x}_1 = -\dot{x}_1 \tag{24}$$

where, x_0 is the constant desired OPDV.

Substituting into Eq. 23, together with Eq. 15, 16 and 17, implies in Eq. 25.

$$\begin{aligned}\sigma\dot{\sigma} = &-\frac{K_T}{J_\Sigma}\varphi_1(k_1z - x)\sigma + (-\frac{\ddot{\lambda}(t)}{\lambda(t)} - \frac{K_T}{J_\Sigma}\varphi_2)x_1\sigma + \\ &(2c_1 - 2\frac{\dot{\lambda}(t)}{\lambda(t)} - \frac{K_T}{J_\Sigma}\varphi_3)x_2\sigma + [f(t) - \frac{K_T}{J_\Sigma}\varphi sgn(\sigma)]\sigma\end{aligned} \tag{25}$$

It is known that the condition for the existence and reachability of a sliding motion is:

$$\dot{V} = \sigma\dot{\sigma} < 0 \tag{26}$$

From Eq. 25 and 26, one can obtain:

$$\varphi_1 = \begin{cases}\alpha_1 > 0 & \text{if} \quad (k_1z - z)\sigma > 0 \\ \beta_1 < 0 & \text{if} \quad (k_1z - z)\sigma < 0\end{cases} \tag{27a}$$

$$\varphi_2 = \begin{cases}\alpha_2 > -\frac{J_\Sigma}{K_T}\frac{\ddot{\lambda}(t)}{\lambda(t)} & \text{if} \quad x_1\sigma > 0 \\ \beta_2 < -\frac{J_\Sigma}{K_T}\frac{\ddot{\lambda}(t)}{\lambda(t)} & \text{if} \quad x_1\sigma < 0\end{cases} \tag{27b}$$

$$\varphi_3 = \begin{cases}\alpha_3 > \frac{2J_\Sigma}{K_T}(c_1 - \frac{\dot{\lambda}(t)}{\lambda(t)}) & \text{if} \quad x_2\sigma > 0 \\ \beta_3 < \frac{2J_\Sigma}{K_T}(c_1 - \frac{\dot{\lambda}(t)}{\lambda(t)}) & \text{if} \quad x_2\sigma < 0\end{cases} \tag{27c}$$

$$\varphi = \begin{cases}\alpha > \frac{J_\Sigma}{K_T}f(t) & \text{if} \quad \sigma > 0 \\ \beta < \frac{J_\Sigma}{K_T}f(t) & \text{if} \quad \sigma < 0\end{cases} \tag{27d}$$

where, $\lambda(t)$ is the time-dependent coefficient defined in Eq. 8. And its first and second order derivatives are followed as:

$$\begin{cases}\dot{\lambda}(t) = \frac{tg(\theta)}{\cos(\theta)} & \frac{\dot{\lambda}(t)}{\lambda(t)} = tg(\theta) \\ \ddot{\lambda}(t) = \frac{1 + \sin^2(\theta)}{\cos^3(\theta)} & \frac{\ddot{\lambda}(t)}{\lambda(t)} = \frac{1 + \sin^2(\theta)}{\cos^2(\theta)}\end{cases} \tag{28}$$

As the characteristics of the VCM, its swing angle which is limited in $\pm 10^\circ$ means that $\dot{\lambda}(t)$ and $\ddot{\lambda}(t)$ are both bounded. If φ_1, φ_2, φ_3 and φ satisfy the inequalities above, the system could meet the general conditions of sliding-mode. It is that the sliding-mode is existent and reachable, also content with the condition of Lyapunov stability, which is $\dot{V} < 0$. Hence, the ISMC system is a global stable system.

After introducing the fuzzy logic control into the ISMC system, the output of the ISMC is modified into Eq. 21. This changes the stability of the system in the Lyapunov approach, but it can be compensated by fuzzy reasoning. According to Rule 1, when $\sigma > 0$ (It is that the

system is moving away the sliding-mode surface), the output of the fuzzy logic control (K_F) is positive, forcing the system to move back to the surface; Rule 2 implies that when $\sigma \approx 0$ (It is that the system is moving on or at the vicinity of the surface), the output of the fuzzy control (K_F) is zero which does not affect the system motion; Rule 3 implies that when $\sigma < 0$ (It is that the system is moving away the sliding-mode surface too), the result is the same as in Rule 1, the system will move back too. Thus, these rules have guaranteed a stable system under all conditions.

SIMULATION AND EXPERIMENTAL RESULTS

The parameters of the VCM and its load in this design are listed in Table 1. The control algorithm has been implemented in the DSP TMS320LF2407. And the effectiveness of the algorithm has been verified by the simulation and experiment results.

Simulation results: Simulations for the double closed-loop control system have been achieved by Synopsys Saber and the fuzzy logic toolbox provided by MATLAB for fuzzy reasoning. The coefficients of proportion and integral for PI in the current loop are $k_p = 2.44$ and $k_i = 0.004$, respectively. Moreover, the parameters for FISMC in the simulation are set as $c_1 = 1180$, $c_2 = 1170$, $k_l = 0.0465$:

Table 1: Parameters of the VCM and the swing arm

Parameter	Name	Value
V_p	Voltage	17 V
I_p	Current	3.4 A
R	DC resistance	5 ohm
L	Inductance	4.4 mH
τ_E	Electrical time constant	0.88 ms
K_T	Torque sensitivity	0.35 Nm A^{-1}
J_m	Coil assembly inertia	9×10^{-5} kg m^2
r	Length of rotary arm	0.135 m
k	Elastic coefficient	1.67 Nm rad^{-1}
J_r	Load torque	0.0182 kg m^2

$$\varphi_1 = \begin{cases} \alpha_1 > 0.13 & \text{if } (k_1 z - z)\sigma > 0 \\ \beta_1 < -0.13 & \text{if } (k_1 z - z)\sigma < 0 \end{cases} \quad \varphi_2 = \begin{cases} \alpha_2 > 0.052 & \text{if } x_1\sigma > 0 \\ \beta_2 < -0.052 & \text{if } x_1\sigma < 0 \end{cases}$$

$$\varphi_3 = \begin{cases} \alpha_3 > 123 & \text{if } x_2\sigma > 0 \\ \beta_3 < -123 & \text{if } x_2\sigma < 0 \end{cases} \quad \varphi = \begin{cases} \alpha > 0.136 & \text{if } \sigma > 0 \\ \beta < -0.136 & \text{if } \sigma < 0 \end{cases}$$

Figure 6 presents a comparison of the motion state of VCM in a single period using FIMSC and PI in speed loop, respectively. The motor swung back and forth in a range of ±9.3° with the voltage input of D.C. 6V. Comparing the angular velocity obtained by using FISMC (wrm(FISMC)) with PI (wrm(PI)), it can be observed that the control performance using FISMC is better than that using PI. There was no overshoot during the startup using FISMC, while there was 33.5% overshoot using PI. Meanwhile, the overshoot during turning around using FISMC is also better than that using PI. The varying of the angular velocity was nonlinear and time-varying, which followed Eq. 7. Its minimum and maximum absolute values of angular velocity (wrm(FISMC)) within one period were 0.23455 rad sec^{-1} (at the equilibrium position of the swing arm) and 0.23715 rad sec^{-1} (at the maximum angle of the arm). Similarly, the motor current (i(FISMC)) was linear with the continuous increasing of the motor angle due to the existence of the flexure pivot, which conformed to Eq. 3. When the arm was at the maximum angle, a large reverse current forced it to slow down and turn back. After turning around, the forward current was used to counterbalance the elastic force of the pivot, ensure the operation of the arm to be stable. Hence, a steep reverse current during turning around is shown in Fig. 6. The maximum absolute value of the instantaneous reverse current was 2.0732 A when it was turning around, while the maximum stable current was only 0.76136 A.

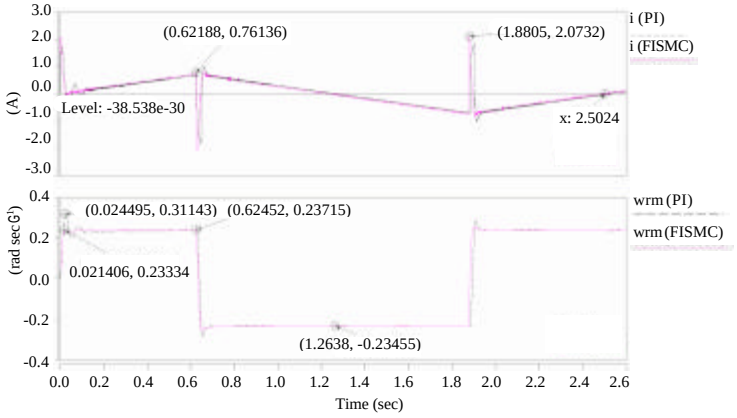

Fig. 6: Simulation results of the motion state of the VCM

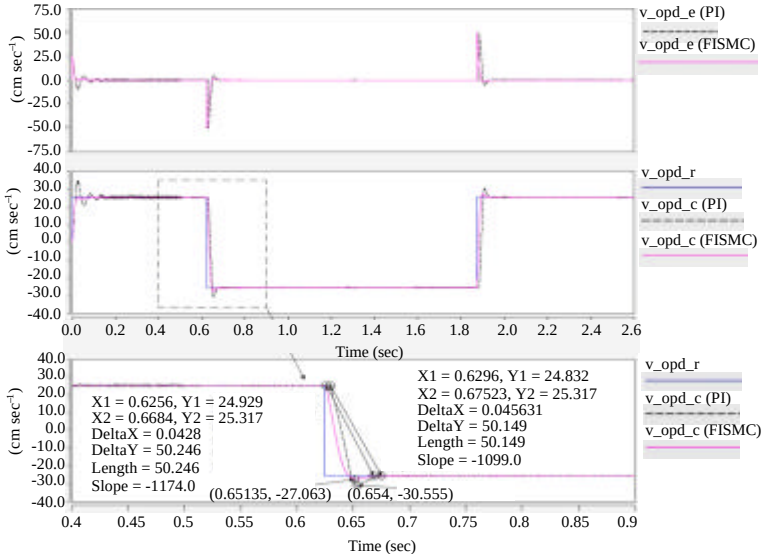

Fig. 7: Simulation results of OPDV in one period and its partial enlarged view of the turning point

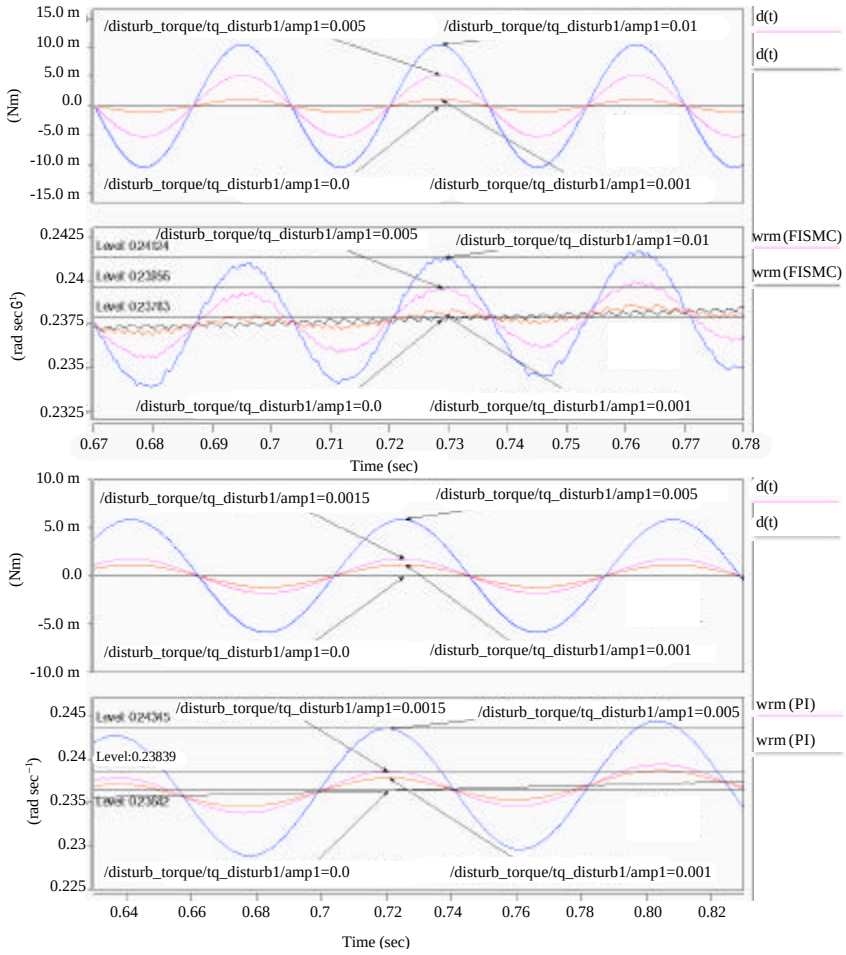

Fig. 8: Simulation results of the angular velocity of the VCM with different inputs of micro-vibration

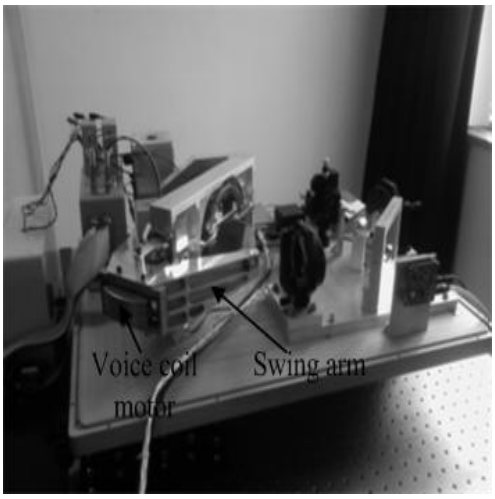

Fig. 9: Experimental platform for FTS

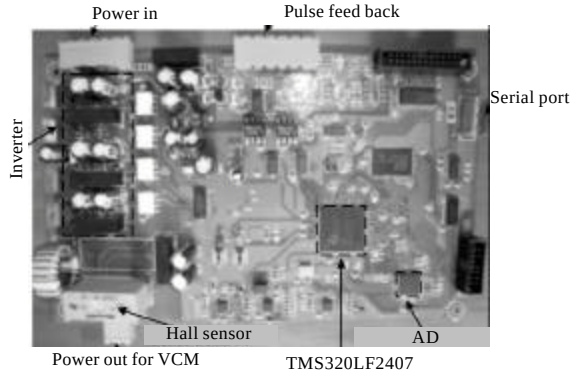

Fig. 10: Control circuit for swing arm

Further more, it was concluded that the operating period of the arm was approximately 2.5024 sec from the time needed for the current returning back to zero.

Comparing the desired OPDV (v_opd_r), its feedback (v_opd_c(FISMC)) and the error (v_opd_e(FISMC)) of OPDV in Fig. 7, it can be concluded that the proposed control algorithm with its parameters set previously is effective in tracking the desired input. The mean square deviation (MSD) of the OPDV was only 0.0895 cm sec^{-1} during the stable range, which meant that the stability of speed was 99.64%. The partial enlarged view of the desired OPDV and its actual feedback at the turning point is shown in the bottom half of Fig. 7. Compared with the performance using PI, it can be obtained that the maximum overshoot of the system response using FISMC at this point was 7.39%, its settling time was about 42.8ms (at a speed stability of 99%), while they were 21.25% and 45.631ms by using PI, respectively.

As the FTS is designed for being applied in spaceborne detecting, a numerical simulation was utilized to analyze the immunity to the micro-vibration disturbance (Bely *et al*., 1993). In Fig. 8, it shows a immunity comparison with the input of micro-vibration disturbance (d(t)) from 0 to 0.01Nm using FISMC and PI, respectively. Observing the responses during the interval of 0.68 to 0.77s, the overshoot of angular velocity was about 0.73% with the input of 0.005Nm micro-vibration disturbance under FISMC, while the overshoot was about 0.83% with the input of 0.0015 Nm disturbance under PI control. In

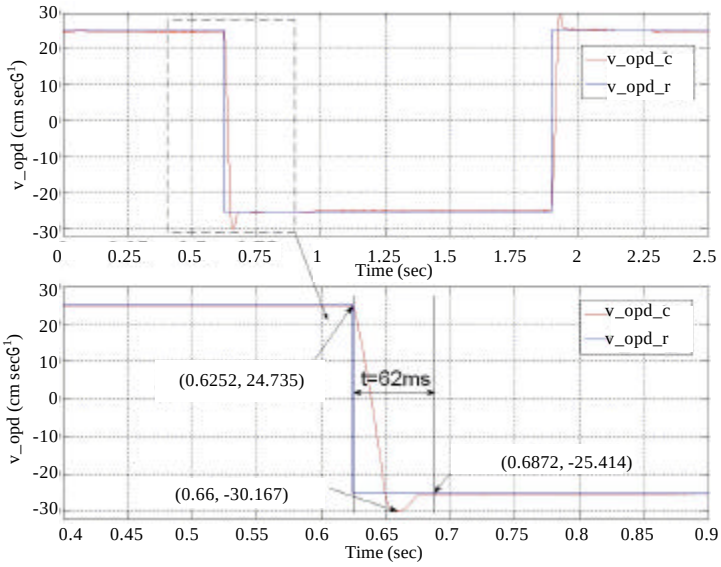

Fig. 11: Experimental results of OPDV and its partial enlarged view of the turning point

other words, the immunity margin using FISMC is better than that using PI.

Simulation results obtained from Saber indicates that the dynamic response of FISMC is faster than that using PI. With the applying of FISMC, the optical path for sampling is expanded, which is equivalent that the resolution is improved. Moreover, a highly stable speed-tracking and robust control for the designed system can be realized.

Experimental results: Experiments were carried out in order to validate the proposed control design and the effectiveness of simulation in this study. The platform for experiment is shown in Fig. 9. The stability of OPDV was tested on the control circuit shown in Fig. 10 with the regulating parameters obtained from simulation. The circuit used a DSP TMS320LF2407 as its controller, and communicated with computer by its serial port. The feedback of OPDV is shown in Fig. 11, drawn by MATLAB with the data from DSP. In the top half of Fig. 11, it shows a comparison of the feedback (v_opd_c) and the desired OPDV (v_opd_r) within one period. The stability of OPDV in the real system was 99.1% during the stable range (except the turning around area). In the bottom half of Fig. 11, it shows the transient response of the feedback at the turning point. The maximum overshoot was 18.8% and the regulation time was 62 ms (corresponding to a stability of 99%).

The experiment results from the realized FTS are consistent with the simulation results. They prove the effectiveness of the proposed design.

CONCLUSION

In this study, a novel control algorithm based on the approach of FISMC for the VCM has been proposed to improve the performance of the FTS. Firstly, the operating principles of the FTS are introduced and the nonlinear time-varying relationship between the feedback of OPDV and angular velocity of the VCM is analyzed. Then, a speed loop based on FISMC and a current loop based on PI control are proposed for the stability of the OPDV and described in detail. The control approach of the ISMC has been applied to eliminate the negative effects of the nonlinear time-varying disturbances caused by the rotary design and the flexure pivot. However, the undesired chattering originated from the ISMC is inevitable. Therefore, a fuzzy logic has been utilized to suppress the chattering intellectually. Furthermore, the stability of FISMC has been proved by the Lyapunov theorem of asymptotic stability. Finally, compared with using PI, simulation results have proved the self-adaptive robustness and rapid response of the system in a theoretical perspective, while the stability of OPDV has been improved to 99.1% in physical implementation based on TMS320LF2407. Further study will be considered to improve the performance of the algorithm during the interval of turning around for responding more rapidly, which could increase the effective OPD for higher spectral resolution.

ACKNOWLEDGMENT

This study was supported by National Natural Science Foundation of China (60834002) and the project named as the development of Michelson interferometer for the FTS from March 2009 to August 2010 in Huazhong University of Science and Technology, Wuhan, China.

REFERENCES

Barambones, O., A.J. Garrido and F.J. Maseda, 2007. Integral sliding-mode controller for induction motor based on field-oriented control theory. IET Control Theory Appl., 1: 786-794.

Bely, P.Y., O.L. Lupie and J.L. Hershey, 1993. Line-of-sight jitter of the hubble space telescope. Proceedings of the SPIE-The International Society for Optical Engineering, April 13-14, Society of Photo-Optical Instrumentation Engineers, Orlando, USA. pp: 55-61.

Chern, T.L. and Y.C. Wu, 1991. Design of integral variable structure controller and application to electrohydraulic velocity servosystems. IEE Proc. D Control Theory Appl., 138: 439-444.

Comolli, L. and B. Saggin, 2005. Evaluation of the sensitivity to mechanical vibrations of an IR fourier spectrometer. Rev. Sci. Instrum., 76: 123112-1-123112-8.

Friedl-Vallon, F., G. Maucher, M. Seefeldner, O. Trieschmann and A. Kleinert *et al.*, 2004. Design and characterization of the balloon-borne michelson interferometer for passive atmospheric sounding (MIPAS-B2). Applied Opt., 43: 3335-3355.

Jiao, Y.P. and F.L. Luo, 2009. An improved sliding mode controller for positive output Luo converter. Proceedings of the 35th Annual Conference of the IEEE Industrial Electronics Society, IECON 2009, Nov. 3-5, IEEE Computer Society, Porto, Portugal, pp: 195-200.

Koshkouei, A.J., K.J. Burnham and A.S.I. Zinober, 2005. Dynamic sliding mode control design. IEE Proc. Control Theory Appl., 152: 392-396.

Lai, C.K. and K.K. Shyu, 2005. A novel motor drive design for incremental motion system via sliding-mode control method. IEEE Trans. Ind. Electron., 52: 499-507.

Morcos, A.C., 1995. Latest developments in voice coil actuators. Power Transm. Des., 37: 67-71.

Spurgeon, S.K., 1991. Choice of discontinuous control component for robust sliding mode performance. Int. J. Control, 53: 163-179.

Steck, T. and T. von Clarmann, 2001. Constrained profile retrieval applied to the observation mode of the michelson interferometer for passive atmospheric sounding. Applied Opt., 40: 3559-3571.

Tao, C.W., M.L. Chan and T.T. Lee, 2003. Adaptive fuzzy sliding mode controller for linear systems with mismatched time-varying uncertainties. IEEE Trans. Syst. Man Cybern. B, 33: 283-294.

Vaughan, A.H., 1989. Imaging michelson spectrometer for hubble space telescope. Proceedings of the Conference on Precision Instrument Design in Conjunction with the Annual Meeting of the Optical Society of America, Nov. 1-3, SPIE, Santa Clara, USA., pp: 2-14.

Wai, R.J. and K.H. Su, 2006. Adaptive enhanced fuzzy sliding-mode control for electrical servo drive. IEEE Trans. Ind. Electron., 53: 569-580.

Wai, R.J., M.A. Kuo and J.D. Lee, 2008. Design of cascade adaptive fuzzy sliding-mode control for nonlinear two-axis inverted-pendulum servomechanism. IEEE Trans. Fuzzy Syst., 16: 1232-1244.

Zachor, A.S., 1977. Drive nonlinearities: Their effects in fourier spectroscopy. Applied Opt., 16: 1412-1424.